Analytical Model and Design Strategy for GaN Vertical Floating Island Schottky Diodes

Xuyang Liu, Sihao Chen, Hang Chen, Yingbin Qiu, and Chao Liu

***Abstract*— We report GaN-based vertical Schottky barrier diodes (SBDs) with embedded floating islands (FIs). The incorporation of FI structure can break the theoretical limit of unipolar vertical GaN devices by homogenizing the electric field distribution within the drift layer. To facilitate comprehensive understanding and structural design of FI SBDs, analytical models for both conducting state and blocking state of GaN FI SBDs are established and verified by TCAD simulation. Parametric optimization for the reverse characteristics of GaN FI SBDs is also carried out systematically. We found that the doping concentration, height of p-GaN FIs, and spacing between adjacent p-GaN FIs are closely associated with the electric field distribution and the reverse breakdown characteristics of vertical FI SBDs. An optimum Baliga's figure of merit (FOM) of 4.98 GW/cm^2 can be achieved, which features a 79.14% enhancement compared with the conventional SBD. The results can provide systematic design guidelines for GaN vertical power electronic systems toward high-voltage, high-speed, and high-power applications.**

***Index Terms*— Analytical model, breakdown voltage, device design, floating island (FI), gallium nitride, specific ON-resistance, vertical Schottky barrier diodes (SBDs).**

I. Introduction

GALLIUM nitride (GaN), featured with unique and superior material properties, such as wide bandgap, high electron mobility, excellent thermal stability, and large critical electrical field, has recently received considerable attention in high-power and high-frequency applications [1], [2]. Therefore, GaN-based power devices are capable of fulfilling the requirements by the next generation of high-power-density and high-efficiency power electronic systems. Specially, GaN Schottky barrier diodes (SBDs), with the merits of high operating frequency, low forward voltage drops, and fast switching speed, stand out among different types of GaN power rectifiers [3], [4]. Currently, both lateral and vertical architectures are being considered for GaN-based SBDs. Lateral GaN SBDs can deliver high switching speed and low ON-resistance owing to high-density two-dimensional electron gas (2DEG) at AlGaN/GaN hetero-interface [5]. Despite the rapid progress in the past two decades, lateral GaN SBDs still face reliability and dynamic issues and are not commercially available so far [6]. On the other hand, the emergence of low-dislocation-density bulk GaN substrates enables the development of vertical GaN-on-GaN SBDs with higher current handling capability, higher breakdown voltage, lower sensitivity to surface trap states, and more efficient chip area utilization compared with lateral SBDs [7].

Nevertheless, similar to their lateral counterparts, GaN vertical SBDs also suffer from large reverse leakage and low reverse blocking capabilities, which limit their application in modern power systems [8]. At present, dislocation density of n-type bulk GaN substrates has been successfully reduced to 10^3–10^6 cm^{-2}, effectively suppressing the dislocation and defect-induced reverse leakage and premature breakdown [9]. Impact ionization under high local electric field and the Schottky-barrier-lowering effect by the image force have become the main factors that restrict the reverse breakdown and leakage characteristics of GaN vertical SBDs. Therefore, it is of utmost significance to regulate the electric field distribution and alleviate the local electric field crowding effect. One of the major obstacles that limit the breakdown capability of GaN vertical SBDs lies in the premature breakdown at the edge of the Schottky anode. Several device architectures have been developed, such as junction barrier Schottky diodes (JBS), merged p-i-n SBDs (MPS), and trench MOS barrier Schottky diodes (TMBS) [10]–[14], which are designed toward a more uniform distribution of electric field near the Schottky junction interface. Note that the majority of the research in the field of GaN vertical power devices focuses on the regulation of electric field at the vicinity of the Schottky surface, while the modulation of electric field distribution within the drift region remains to be explored and investigated.

Typical drift region engineering techniques involves the adoption of "super junction" (SJ) [15] and "floating island" (FI) structures. The SJ structures were first proposed and have been extensively verified in Si-based power devices to be

Manuscript received March 11, 2022; accepted April 22, 2022. Date of publication May 11, 2022; date of current version May 24, 2022. This work was supported in part by the National Natural Science Foundation of China under Grant 62104135, in part by the Shenzhen Science and Technology Program under Grant JCYJ20210324141212030, in part by the Guangdong Basic and Applied Basic Research Foundation under Grant 2020A1515111018, in part by the Shandong Provincial Natural Science Foundation under Grant ZR2020QF079, and in part by the Qilu Young Scholar program under Grant 11500089963075. The review of this article was arranged by Editor M. Meneghini. *(Corresponding author: Chao Liu.)*

Xuyang Liu, Sihao Chen, Hang Chen, and Chao Liu are with the State Key Laboratory of Crystal Materials, Shandong Technology Center of Nanodevices and Integration, School of Microelectronics, Institute of Novel Semiconductors, Shandong University, Jinan 250100, China, and also with the Shenzhen Research Institute, Shandong University, Shenzhen 518057, China (e-mail: chao.liu@sdu.edu.cn).

Yingbin Qiu is with Crosslight Software Inc., Shanghai 200063, China.

Color versions of one or more figures in this article are available at https://doi.org/10.1109/TED.2022.3171733.

Digital Object Identifier 10.1109/TED.2022.3171733

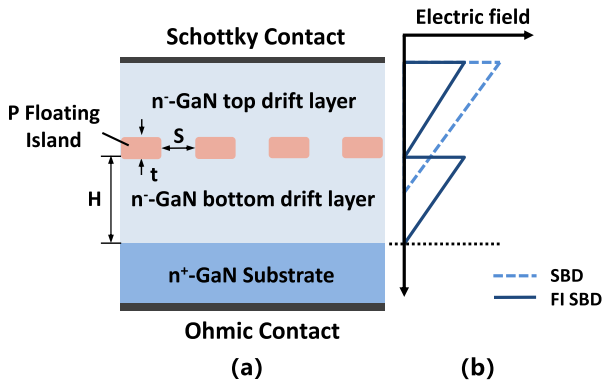

Fig. 1. (a) Schematic cross section of the GaN-based SBD with p-GaN FIs. (b) Electric field distribution of the conventional SBD and FI SBD at identical reverse bias.

effective in circumventing the one-dimensional (1-D) unipolar material limit. But for GaN power devices, it is particularly challenging to realize high-quality vertical SJ structures owing to the immature fabrication technology to form the deep n- and p-doped pillars in the GaN drift layers [16]. Moreover, the difficulty in exact control of the doping levels in GaN hinders the realization of the charge-balanced condition in the alternating vertical pillars, which is highly desired for GaN vertical SJ devices. On the other hand, the fabrication process for FI structures is much less complexed. The buried p-type islands are much thinner compared with the SJ pillars and can be simply formed by a few runs of etching-epitaxy or implantation-epitaxy processes. Hence, the FI structure can serve as an alternative solution for engineering electric field distribution in the drift region. Recently, Ghandi *et al.* [17], [18] experimentally demonstrated improved breakdown characteristics in silicon carbide (SiC) power devices by incorporating buried p-doped FIs inside the drift layer, which proves the feasibility of fabricating FI SBDs. So far, there is no report about the application of FI structure in GaN vertical SBDs, and a systematic optimization strategy to reveal device physics is still lacking.

In this article, we report for the first time GaN vertical SBDs with embedded p-GaN FIs, for the purpose of engineering the electric field distribution in the drift layer, toward an enhanced breakdown voltage of GaN vertical SBDs. The article is organized as follows. In Section II, the device architectures and working principles of FI SBDs are introduced. In Section III, the analytical models for both conducting state and blocking state are established to analyze the effect of the main design parameters of FI SBDs. TCAD simulation is conducted to examine the effectivity of the analytical models. In Section IV, we further investigate the influence of the key structural parameters by two-dimensional (2-D) simulation on electric field profiles and breakdown voltage for FI SBDs. Finally, this article is concluded in Section V.

II. Device Architectures and Principles

The schematic of FI SBDs is shown in Fig. 1(a). The structure features a 15-μm-thick-n$^-$-GaN drift layer (Si $= 2 \times 10^{16}$ cm^{-3}) on a 2-μm-thick-n$^+$-GaN substrate

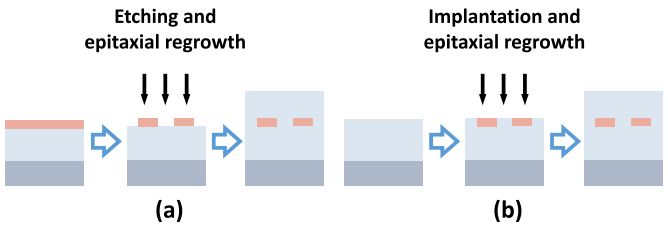

Fig. 2. Schematic process flows for (a) etching-epitaxy process and (b) implantation-epitaxy process.

(Si $= 5 \times 10^{18}$ cm^{-3}), except that p-GaN FIs are incorporated in the drift region of FI SBDs. The impact of the following parameters on the device performance are investigated and analyzed to fully explore the working mechanism of FIs by varying the background doping concentration (N_D), p-GaN doping concentration (N_p), height of p-GaN FIs (H), and spacing between adjacent p-GaN FIs (S).

For an unambiguous explanation of the mechanism behind electric field regulation by the embedded p-GaN FIs, 1-D electric field distributions are extracted for the conventional and FI SBDs. As shown in Fig. 1(b), the peak electric field of the conventional SBD structure occurs at the Schottky surface, producing a nonuniform triangular electric field distribution in the drift layer. As a result, the average achievable electric field in the drift region is far less than the GaN material limit under reverse bias condition. With embedded FIs in the drift region, a more uniform double-triangular distribution can be observed for the electric field profile. At identical reverse bias, the peak electric field value can be effectively reduced for FI SBDs, compared with that in the conventional SBDs. As a result, the average achievable breakdown field value in the drift region can be effectively enhanced and the reverse blocking capability can be efficiently boosted. Furthermore, the FI structure allows the design of a drift layer with a higher doping concentration without degrading the breakdown characteristics, which can result in a reduced ON-resistance and break the theoretical limit of the unipolar GaN vertical Schottky diodes.

To realize such a sandwiched structure with p-type FIs incorporated in the n-type drift layer, two techniques can be taken into account, which are etching-epitaxy process and implantation-epitaxy process, as shown in Fig. 2. The etching-epitaxy process flow includes the growth of a p-i-n structure, followed by selective etching to create isolated p-GaN islands on the bottom n-GaN layers, and subsequent regrowth of the top n-GaN drift layer to complete the full epitaxial structure. Similar to the etching-epitaxy process, the implantation-epitaxy technique also features a two-step epitaxial growth process, except that the selective p-doping in the drift layer is realized by ion implantation. Both the etching-epitaxy and implantation techniques have been developed and adopted in the fabrication of a variety of GaN-based devices [19]–[21]. Recently, vertical GaN devices with selective p-GaN filling have been successfully achieved [22], [23], demonstrating the feasibility of the proposed fabrication process. However, the effectiveness of FI structure is still hindered by the challenges in precise control of selective

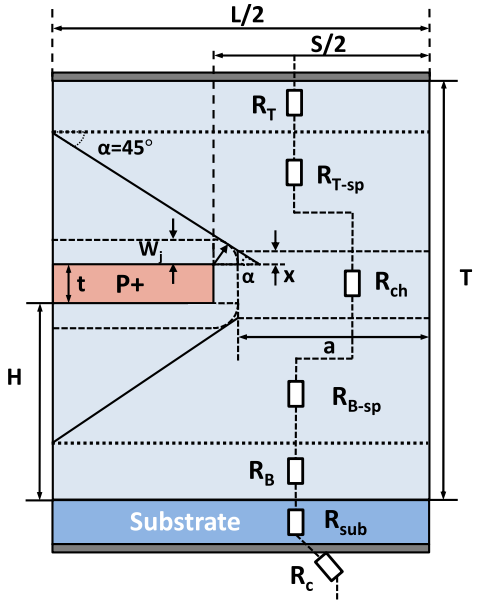

Fig. 3. Specific ON-resistance structure model of GaN FI SBDs.

p-doping and efficient acceptor activation. A thorough development and optimization is highly desired to fully exploit the potential of FI structure.

For the purpose of obtaining a comprehensive understanding of the working principles of FI SBDs, the analytical models for the blocking and conducting states of the devices are established by quantitatively calculating the electric field distribution and the carriers' transport behavior in the drift region. TCAD simulations are carried out using Advanced Physical Models of Semiconductor Devices (APSYS) software to verify the models. The physical models include continuity and Poisson's equations. The breakdown of the device is handled by the impact ionization model, which determines the carrier generation rate during the carrier multiplication process. The carrier generation rate in the avalanche breakdown condition is described by the equation below

$$G = \alpha_n J_n + \alpha_p J_p \tag{1}$$

where α_n and α_p are the impact ionization coefficients for electrons and holes, respectively, and J_n and J_p are the electron and hole current densities, respectively. The impact ionization coefficient defines the number of electron–hole pairs that are generated by one single electron or hole per unit distance.

III. Analytical Models for FI Structure

A. Conducting State Model

To interpret the forward conduction principle of FI SBDs, we established an analytical resistance model based on a unit cell with stripe geometry, as shown in Fig. 3. The specific ON-resistance ($R_{\mathrm{ON,sp}}$) of FI SBDs can be expressed as

$$R_{\mathrm{ON,sp}} = R_{T,\mathrm{sp}} + R_{B,\mathrm{sp}} + R_{\mathrm{SP,sp}} + R_{\mathrm{CH,sp}} + R_{\mathrm{SUB,sp}} + R_{C,\mathrm{sp}} \tag{2}$$

where $R_{T,\mathrm{sp}}$ and $R_{B,\mathrm{sp}}$ represent the specific resistance of the top and bottom drift layers, respectively. $R_{\mathrm{SP,sp}}$ is composed of $R_{T-\mathrm{sp,sp}}$ and $R_{B-\mathrm{sp,sp}}$, which are the top and bottom specific spreading resistances, respectively. $R_{\mathrm{CH,sp}}$ is the specific channel resistance [24]. On account of the fact that the specific substrate resistance ($R_{\mathrm{SUB,sp}}$) and the specific cathode contact resistance ($R_{C,\mathrm{sp}}$) can be neglected, the overall $R_{\mathrm{ON,sp}}$ can be simplified by

$$R_{\mathrm{ON,sp}} = R_{T,\mathrm{sp}} + R_{B,\mathrm{sp}} + R_{\mathrm{SP,sp}} + R_{\mathrm{CH,sp}} \tag{3}$$

The formulas of $R_{T,\mathrm{sp}}$, $R_{B,\mathrm{sp}}$, $R_{\mathrm{SP,sp}}$, and $R_{\mathrm{CH,sp}}$ can be acquired as follows:

$$R_{T,\mathrm{sp}} = \rho\left[T - H - t - x - \left(\frac{L}{2} - a\right)\right] \tag{4}$$

$$R_{B,\mathrm{sp}} = \rho\left[H - x - \left(\frac{L}{2} - a\right)\right] \tag{5}$$

$$R_{\mathrm{SP,sp}} = 2R_{T-\mathrm{sp,sp}} = 2R_{B-\mathrm{sp,sp}} = L \cdot \rho \int_0^{\left(\frac{L}{2}-a\right)} \frac{1}{a+y} dy \tag{6}$$

$$R_{\mathrm{CH,sp}} = \rho\left[(t + 2x) \cdot \frac{L}{2a}\right] \tag{7}$$

where T is the total thickness of the drift layer, L is the width of the whole unit cell, H is the height of the p-GaN FIs, which equals the thickness of the drift layer underneath FIs, t is the thickness of the FI structure, and a and x are the parameters used to simplify calculations and can be, respectively, given by

$$a = \frac{S}{2} - W_j \tag{8}$$

$$x = \left(\frac{1 - \sin\alpha}{\sin\alpha}\right) W_j \tag{9}$$

The value of α is equal to 45° for p-n junction and W_j is the p-n junction depletion width induced by build-in potential, derived from the following equation

$$W_j = \frac{\varepsilon_s}{qN_n} \sqrt{\frac{2k'T' \ln\frac{N_n N_p}{n_i^2}}{\frac{\varepsilon_s}{q}\left(\frac{1}{N_n} + \frac{1}{N_p}\right)}} \tag{10}$$

Here, n_i is the intrinsic carrier concentration, k' is Boltzmann's constant, and T' is the temperature.

The resistivity of the drift region ρ can be expressed as

$$\rho = \frac{1}{N_D q \mu} \tag{11}$$

where N_D is the doping concentration of the drift region. The model for the doping-concentration-dependent electron mobility [25] is given as follows

$$\mu = \mu_{\min} + \frac{\mu_{\max} - \mu_{\min}}{1 + \left(\frac{N_D}{N_{\mathrm{ref}}}\right)^{\beta}} \tag{12}$$

Here, μ is the electron mobility of the drift layer, $\mu_{\max} = 1460.7$ cm^2/(V·s), $\mu_{\min} = 295$ cm^2 /(V·s), $N_{\mathrm{ref}} = 1 \times 10^{17}$ cm^{-3}, and $\beta = 0.66$.

Based on the resistance model above, we calculated each component of $R_{\mathrm{ON,sp}}$ of FI SBDs with different p-GaN spacing,

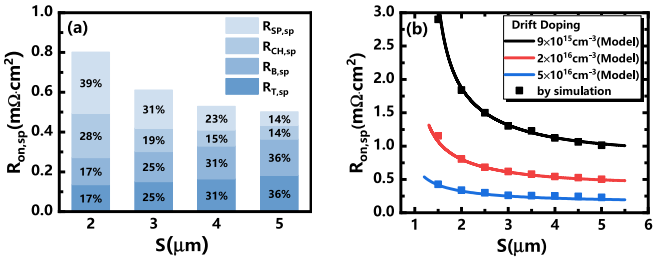

Fig. 4. (a) Component and proportion of the specific ON-resistance variations with S. (b) Comparison between the calculation results from the analytical models and the simulation results for $R_{ON,sp}$.

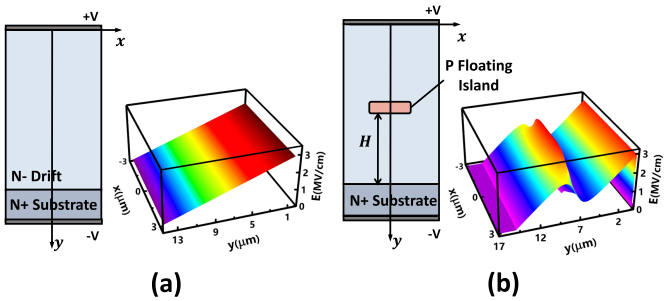

Fig. 5. Schematic cross sections and 2-D electric field distribution of (a) conventional SBD and (b) FI SBD.

as shown in Fig. 4(a). With a narrow spacing of 2 μm, the dominant factors that influence $R_{ON,sp}$ are the FI-dependent components ($R_{CH,sp} + R_{SP,sp}$), which account for 67% of the total resistance. The proportion drops to 28% with the spacing increased to 5 μm, indicating that the resistance of the top and bottom parts of the drift layer ($R_{T,sp}$+$R_{B,sp}$) starts to dominate.

We further investigated the effect of the spacing between p-GaN structures on the forward characteristics of FI SBDs, under different background doping concentrations in the drift region, as shown in Fig. 4(b). The simulated $R_{ON,sp}$(scatters) of FI-SBDs by TCAD simulation is also presented and compared with the calculated values (solid lines). An excellent agreement indicates high accuracy and effectiveness of the proposed model. A higher background doping concentration is favorable for a lower $R_{ON,sp}$, thanks to the reduced resistivity (ρ) of the drift region. Moreover, the spacing between adjacent p-GaN FIs is also closely associated with $R_{ON,sp}$ of FI SBDs. With decreased spacing, a monotonous increase in $R_{ON,sp}$ can be observed. Note that with a decreased spacing from 5 μm to 2 μm, FI SBDs with a background doping concentration of 2×10^{16} cm^{-3} only exhibited a marginal increase in $R_{ON,sp}$ from 0.5 mΩ·cm^2 to 0.81 mΩ·cm^2, which demonstrates the feasibility of improving the breakdown characteristics by reducing FI spacing, without degrading the forward performance significantly.

B. Blocking State Model

Fig. 5(a) and (b) illustrates the schematic structure and 2-D electric field distribution for the conventional SBD and FI SBD. While the conventional planar SBD featured a single electric field peak at the Schottky contact, two electric field peaks can be observed for FI SBDs, which effectively

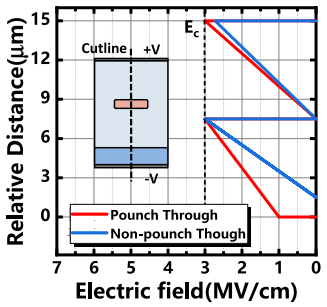

Fig. 6. Electric field distribution along the cutline for PT and NPT types. (Inset: cross section of FI structure for calculation of breakdown voltage.)

enhanced the average achievable electric field value in the drift region and boosted the breakdown performance. In the meantime, the 2-D electric field is identically aligned along the x-direction, making it possible to simplify the breakdown analysis with a 1-D approximation model in the y-direction. Hence, the breakdown voltage of FI SBDs can be defined as the voltage when the maximum $E(y)$ reaches the critical electric field (E_{cr}), which can be derived as [26]

$$E_{cr} = \frac{2.162\times10^6 + T\times800\ \mathrm{K}^{-1}}{1 - \frac{1}{4}\log_{10}\left(N_d/10^{16}\ \mathrm{cm}^{-3}\right)}\ \mathrm{V/cm} \tag{13}$$

where T is the temperature in Kelvin, and N_D is the doping concentration of the drift region.

To investigate the breakdown mechanism using the 1-D approximation model, we extract the schematic electric field profiles of FI SBDs, along the dashed line in the inset of Fig. 6. Subject to different design parameters, FI SBDs can exhibit punchthrough (PT) or non-punchthrough (NPT) behaviors under reverse bias condition, as shown by the red and blue lines, respectively. The PT condition corresponds to the case when the bottom drift region is fully depleted, and thus the bottom electric field follows a trapezoid distribution. On the contrary, the NPT case happens when the bottom part of the drift layer is thicker than the depletion width under reverse bias condition, resulting in a triangular shape of electric field. Therefore, subsequent calculation of the breakdown voltage will be implemented in two cases, i.e., the PT condition and NPT condition, respectively.

The breakdown voltage of FI SBDs can be estimated by the integral of 1-D electric field profiles, which consists of the electric field at the top region (E_T) and the bottom region (E_B):

$$V_{BV} = \int (E_T(y) + E_B(y))dy \tag{14}$$

To take full advantage of the FIs and protect the Schottky junction from premature breakdown, the FI SBD structure should be designed in such a way that the breakdown occurs underneath FIs. Therefore, the breakdown voltage of FI SBD is calculated under the assumption that the peak value of the electric field at the bottom of the FI structures reaches the critical electric field of GaN materials. As a result, the electric field at the top region (E_T) can be obtained as

$$E_T(y) = \frac{qN_D}{\varepsilon_s}(T - t - H - y), \quad y \le T - t - H \tag{15}$$

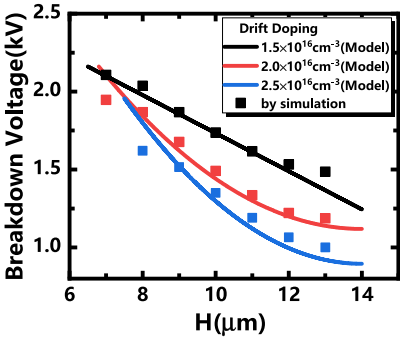

Fig. 7. Comparison between the calculation results from the analytical models and the simulation results for breakdown voltage.

The electric field value at the bottom region (E_B) under the NPT condition can be expressed as

$$E_B(y) = E_{cr} - \frac{qN_D}{\varepsilon_s}(y - T + H)$$
$$T - H \le y \le \frac{E_{cr}\varepsilon_s}{qN_D} + T - H \quad (16)$$

Comparatively, under the PT condition, the electric field at the bottom region (E_B) is

$$E_B(y) = E_{cr} - \frac{qN_D}{\varepsilon_s}(y - T + H), \quad T - H \le y \le T \quad (17)$$

By calculating the integral for 1-D electric field profiles, the breakdown voltage of FI SBDs can be obtained. To verify the analytical models presented above, we calculated the breakdown voltage of FI SBDs and compared the results with those from TCAD simulation, as shown in Fig. 7. The calculated results with the analytical models are shown by the solid lines, while the simulated results are depicted by scatters. A good agreement can be observed between the calculated and simulated results, regarding the value and tendency. More detailed discussion on the reverse characteristics is presented in Section IV.

IV. Optimization of the FI Structure

A. Impact of P-doping Concentration on the Electrical Properties of GaN FI SBDs

To fully understand the working principle of FIs, the influence of p-doping concentration (acceptor concentration) on the reverse characteristics is investigated under different background doping levels, as shown in Fig. 8(a). The breakdown voltage of the conventional planar SBDs with the corresponding background doping levels is also labeled for comparison, and the breakdown voltage is extracted when the reverse leakage current density reaches 0.1 A/cm^2. We first look into the FI SBDs with a background doping concentration of 2×10^{16} cm^{-3}, which is most commonly adopted for the drift region of GaN vertical power devices [27]. The p-doping concentration of FIs exhibited a significant influence on the reverse breakdown voltage of FI SBDs. As the p-doping concentration of FIs increases, the reverse breakdown voltage first increases and then decreases before saturation. A maximum breakdown voltage of 1956 V can be observed with

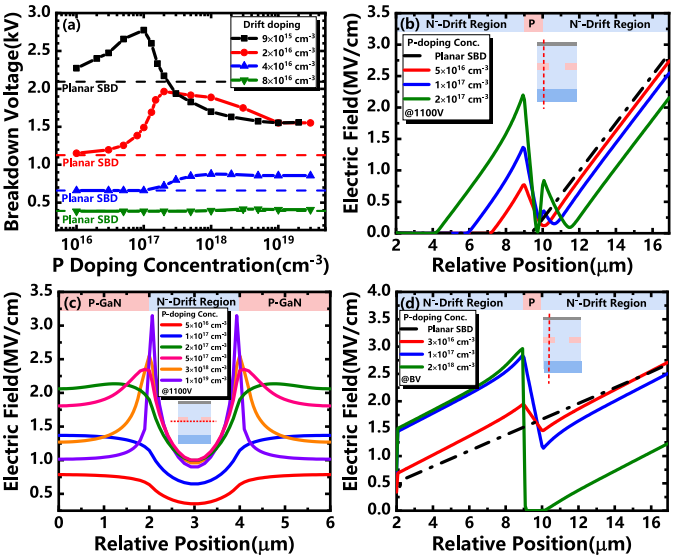

Fig. 8. (a) Breakdown voltage as a function of p-doping concentration for FI SBDs with different drift layer doping concentrations. (b) Electric field profiles along the midline of FI when the reverse bias is 1100 V (n$^-$-GaN drift doping concentration: 2×10^{16} cm^{-3}). (c) Electric field profiles at the bottom of FIs with different p-doping concentrations. (d) Electric field profiles along the midline of FI under breakdown (n$^-$-GaN drift doping concentration: 9×10^{15} cm^{-3}).

a p-doping concentration of 2×10^{17} cm^{-3}, which is 73.6% larger than that of the conventional planar SBD without FIs (1127 V).

Further decreasing the background doping concentration to 9×10^{15} cm^{-3} can result in an even larger peak breakdown voltage of FI SBDs (2775 V) with a p-doping concentration of 1×10^{17} cm^{-3} with a lower background doping concentration. However, with a p-doping concentration exceeding 2×10^{17} cm^{-3}, the embedded p-islands exhibit an adverse impact on the reverse characteristics of FI SBDs and result in a remarkably lower breakdown voltage than that of the conventional SBDs. Subject to a background doping concentration higher than 4×10^{16} cm^{-3}, the embedded p-FIs appear to be deactivated and limited improvement can be observed, compared with the conventional planar SBDs. This can be attributed to the fact that the peak electric field underneath the Schottky contact already reaches the critical value before the depletion layer extends to the FI structure, and thus premature breakdown occurs at the surface. Therefore, the breakdown voltage of FI SBDs is nearly consistent with the conventional planar device, denoting an ineffective role of FIs.

To investigate the influencing mechanisms of p-doping concentration on the reverse characteristics of FI SBDs, we extracted the vertical electric field profiles along the midline of the p-type islands at a reverse bias of 1100 V, as shown in Fig. 8(b). The conventional planar SBDs with a background doping concentration of 2×10^{16} cm^{-3} exhibit a single triangular-shaped electric field profile, which is generally regarded as one of the bottlenecks that limit the breakdown characteristics of GaN SBDs. By incorporating p-type FIs in the drift region, the electric field profile can be engineered toward a quasi-double peak distribution, due to the additional depletion effect from the embedded p-n junction between

p-type FIs and n-type drift region. With increased p-doping concentration from 5×10^{16} cm^{-3} to 2×10^{17} cm^{-3}, a transfer of the electric field can be observed from the Schottky interface to the bottom of FIs. The decreased electric field at the Schottky junction is beneficial to reduce the reverse leakage caused by the barrier lower effect under the condition of excessive electric field, and favorable to avoid premature breakdown at the Schottky junction, which can well-explain the monotonous increase in the breakdown voltage with relatively lower p-doping concentration in Fig. 8(a).

In addition to the vertical distribution, the lateral electric field profiles are also plotted along the bottom interface of FIs, as shown in Fig. 8(c). In the low p-doping range from 5×10^{16} cm^{-3} to 2×10^{17} cm^{-3}, the electric field is evenly distributed without spikes and the average value gradually increases with p-doping concentration, which agrees with the results observed in Fig. 8(b). Further increase in the p-doping concentration to above 2×10^{17} cm^{-3} leads to a lateral redistribution of the electric field, in which the electric field gradually concentrates at the corner of FIs. The locally crowded electrical field at the corner of FI structures leads to premature breakdown of the devices, which addresses the decrease in the breakdown with a relatively higher p-doping in Fig. 8(a).

To figure out the breakdown mechanism of FI SBDs with a relatively low background concentration of 9×10^{15} cm^{-3}, we plotted the vertical electric field profiles along the midline of FIs at the breakdown voltages of the devices, as presented in Fig. 8(d). Note that the electric field profile of the conventional planer SBDs exhibits a trapezoidal shape, indicating a PT condition for the devices. Under the circumstances, the effect of FIs on the electric field profiles and reverse characteristics of SBDs can behave differently from that under NPT conditions. With a low p-doping concentration of 3×10^{16} cm^{-3} in FIs, the breakdown still occurs at the Schottky junction. The small hump in the profile indicates an additional blocking capability provided by FIs, which results in a minor improvement in the breakdown voltage. By increasing the doping concentration to 1×10^{17} cm^{-3}, a more uniformly distributed double-peak electric field profile can be recorded at the moment of breakdown, producing the maximum integral area and the largest breakdown voltage. Nevertheless, with a higher doping concentration of 2×10^{18} cm^{-3}, the electric field value in the upper part of FI SBDs is much lower than the critical field of the GaN material, which means the drift region above FIs fails to hold the reverse voltage effectively, resulting in premature breakdown at an even lower voltage than that of the conventional planar SBDs. Based on the analysis above, the p-doping concentration of FIs can exert an enormous implication on the electric field profiles of FI SBDs, which directly determines the breakdown characteristics of the devices.

B. Impact of p-GaN Height on the Electrical Properties of GaN FI SBDs

Except for p-doping concentration, the height of FIs (H) also plays a crucial role in the reverse characteristics of FI SBDs, as illustrated in Fig. 9(a). A similar phenomenon can

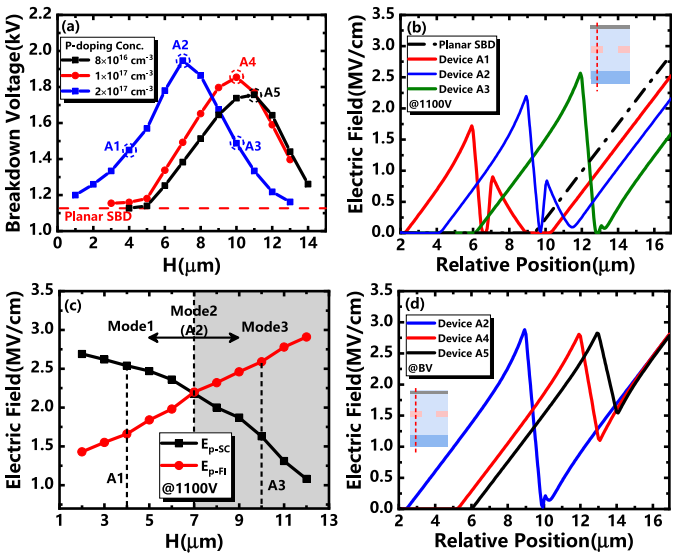

Fig. 9. (a) Breakdown voltage as a function of the height of FIs (H) in FI SBDs with different p-doping concentrations. (b) Electric field profiles along the midline of FI when the reverse bias is 1100 V. (c) Electric field peak at the Schottky contact ($E_{p\text{-}SC}$) and the bottom of FIs ($E_{p\text{-}FI}$) with p-doping concentration of 2×10^{17} cm^{-3} when the reverse bias is 1100 V. (d) Electric field profiles along the midline of FIs at breakdown voltage.

be observed for FI SBDs, in which the reverse breakdown voltage first increases and then decreases with increased height of FIs. With the p-doping concentration increased from 8×10^{16} cm^{-3} to 2×10^{17} cm^{-3} in the FIs, the peak value of the breakdown voltage increases from 1757 V to 2062 V, while the optimal height of FIs to achieve the maximum breakdown decreases from 11 μm to 7 μm.

For the purpose of analyzing and elucidating the trend above, we intercepted the electric field profile along the midline of FIs at a reverse bias of 1100 V, as shown in Fig. 9(b). Devices A1–A3 are selected with identical structures and parameters except the height of FIs. Compared with the conventional planar SBDs, Device A1 features a minor reduction in the electric field at the Schottky interface. In the meantime, an extra peak of the electric field occurs in the vicinity of FIs, revealing an additional reverse blocking capability provided by the embedded FIs. Therefore, Device A1 exhibits a slightly increased breakdown voltage, when compared with the conventional planar SBDs. However, the electric field at the Schottky junction is still larger than that beneath FIs, indicating insufficient screening effect of the electric field by the embedded FIs. By increasing the FI height to 7 μm in Device A2, the electric field in FI SBDs is further redistributed toward a more balanced condition with an almost identical electric field value at the Schottky and the FI interface, corresponding to the maximum breakdown voltage achieved in Device A2. Nevertheless, when we further increase the height of FIs to 11 μm (Device A3), the electric field under FIs overwhelms that at the Schottky interface, which results in premature breakdown at FIs and addresses the decrease in the breakdown with a relatively higher FI in Fig. 9(a).

To intuitively illustrate the redistribution process of sthe electric field with different heights of FIs, we extract the peak electric field value from the Schottky (E_{p-SC}) and the FI

(E_{p-FI}) interfaces of FI SBDs, as shown in Fig. 9(c). With increased FI height, the peak electric field in FI SBDs is gradually transferred from the Schottky contact to the bottom of FIs. Correspondingly, the breakdown behaviors of FI SBDs can be described by three modes, including mode 1 (breakdown at the Schottky junction), mode 2 (simultaneous breakdown at the Schottky junction and FIs), and mode 3 (breakdown at the Schottky junction). Specially, mode 2, with an FI height of 7 μm, features the most uniform distribution ($E_{p-SC} = E_{p-FI}$) and corresponds to the optimal breakdown voltage (Device A2) in Fig. 9(a). Therefore, we can come to the design strategy that the optimum breakdown characteristics of FI SBDs can be obtained by adjusting the FI height toward a uniformly distributed electric field profile (mode 2).

Subject to different p-doping concentrations in FIs, the optimal FI height to achieve the highest breakdown also varies. To interpret the variation in the peak position and value of the breakdown voltage with different p-doping concentrations, the electric field profiles are plotted along the midline of FIs at breakdown voltage in Fig. 9(d). Devices A2, A4, and A5 represent FI SBDs featuring the largest breakdown voltage with p-doping concentrations of 8×10^{16} cm^{-3}, 1×10^{17} cm^{-3}, and 2×10^{17} cm^{-3}, respectively. Uniformly distributed electric field profiles ($E_{p-SC} = E_{p-FI}$) can be observed in all the three devices, effectively verifying the proposed design strategy above. Note that a larger FI height is required to achieve mode 2 for FI SBDs with a lower p-doping concentration, which agrees with the results from Fig. 9(a). In addition, thanks to the larger p-doping concentration and smaller height of FIs, an increased depletion width and thus enhanced breakdown performance can be observed from Devices A5 to A2.

C. Impact of Spacing Between Adjacent p-GaN FIs on the Electrical Properties for GaN FI SBDs

After addressing the impact of p-doping concentration and FI height on the breakdown performance of FI SBDs, we then investigate how the spacing (S) between adjacent FIs affects the electric field distribution and the breakdown voltage of FI SBDs. Note that the spacing should be designed in such a way that the channel region between FIs are not pinched off at zero or forward bias to assure a sufficient current flow. As shown in Fig. 10(a), the breakdown voltage of FI SBDs decreases monotonously with increased spacing at all listed p-doping concentrations.

To investigate the influence of spacing on the breakdown characteristics of FI SBDs, we extract the electric field profiles for Devices B1–B4 at a reverse bias of 1100 V. Fig. 10(b) shows plots of the vertical electric field profiles along the midline of FI for the device with different spacings. With decreased spacing from Devices B1 to B4, the surface electric field underneath the Schottky contact reduces and the peak electric field at the bottom of FIs increases before saturation. Note that an almost identical electric field value at the Schottky and the FI interface can be observed for Device B4, indicating that the device behavior follows mode 2, and thus the maximum breakdown voltage can be achieved.

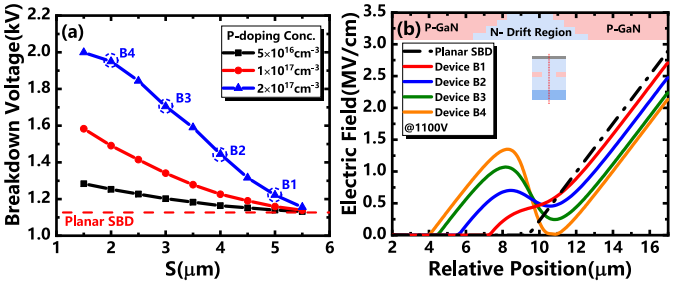

Fig. 10. (a) Breakdown voltage as a function of spacing (S) between adjacent FIs in FI SBDs with different p-doping concentrations. (b) Electric field profiles along the midline of FI with p-doping concentration of 2×10^{17} cm^{-3} when the reverse bias is 1100 V.

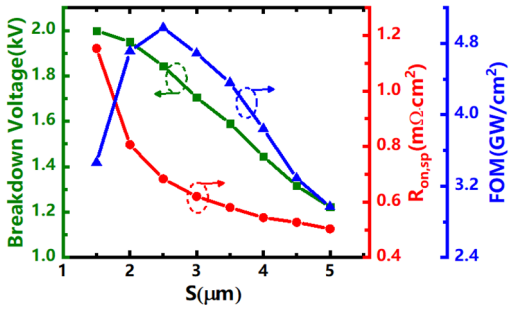

Fig. 11. Extracted $R_{ON,sp}$, BV, and FOM as a function of spacing (S) between adjacent FIs in FI SBDs.

Meanwhile, increased depletion width underneath FIs also explains the enhanced breakdown voltages with decreased FI spacing. Based on the analysis above, we can conclude that a relatively smaller S can produce a more even distribution in the vertical and lateral electric field distribution, thus enhancing the breakdown characteristics of FI SBDs.

Based on the modeling and simulation results obtained above, we extracted the breakdown voltage and specific ON-resistance with different spacing (S) between adjacent FIs, as presented in Fig. 11. Moreover, we calculated and compared Baliga's figure of merit (FOM) for GaN FI SBDs which can represent the comprehensive performance of the devices by taking the trade-off issues into consideration. The FOM shows a trend of initially increasing and then decreasing as the spacing (S) increases. A maximum FOM value of 4.98 GW/cm^2 can be obtained with a spacing of 2.5 μm, which features a 79.14% enhancement compared with the conventional SBD.

Several researches have reported that FI device with p-doped islands inside the drift region exhibits turn-on hysteresis and significant dynamic loss on account of slow carrier generation–recombination rate during transition between blocking and conduction [28]. To alleviate this drawback, intermittent vertical p-type pillars (P-Bus) can be implemented to supply holes from the top contact to the buried p-doped islands [28], [29].

V. Conclusion

In summary, we report GaN SBDs with embedded p-GaN FIs and establish the analytical models for both conducting and

blocking states for the GaN-based FI SBDs. The incorporation of FIs can modulate the electric field distribution in the drift region, dramatically enhancing the FOM by 79.14% to 4.98 GW/cm^2. We believe that the results are very promising to boost further application of GaN vertical Schottky diodes for the next generation of high-power and high-efficiency power electronic systems.

Acknowledgment

The authors would like to thank R. A. Khadar, H. Wang, and J. Yin for their valuable discussion and technical support.

References

[1] H. Ohta *et al.*, "Vertical GaN p-n junction diodes with high breakdown voltages over 4 kV," *IEEE Electron Device Lett.*, vol. 36, no. 11, pp. 1180–1182, Nov. 2015, doi: 10.1109/LED.2015.2478907.

[2] Y. Zhang *et al.*, "High-performance 500 V quasi- and fully-vertical GaN-on-Si p-n diodes," *IEEE Electron Device Lett.*, vol. 38, no. 2, pp. 248–251, Feb. 2017, doi: 10.1109/LED.2016.2646669.

[3] Y. Li *et al.*, "Quasi-vertical GaN Schottky barrier diode on silicon substrate with 1010 high on/off current ratio and low specific on-resistance," *IEEE Electron Device Lett.*, vol. 41, no. 3, pp. 329–332, Mar. 2020, doi: 10.1109/LED.2020.2968392.

[4] M. Xiao *et al.*, "5 kV multi-channel AlGaN/GaN power Schottky barrier diodes with junction-fin-anode," in *IEDM Tech. Dig.*, Dec. 2020, p. 5, doi: 10.1109/IEDM13553.2020.9372025.

[5] M. Xiao, Y. Ma, K. Liu, K. Cheng, and Y. Zhang, "10 kV, 39 mΩ·cm^2 multi-channel AlGaN/GaN Schottky barrier diodes," *IEEE Electron Device Lett.*, vol. 42, no. 6, pp. 808–811, Jun. 2021, doi: 10.1109/LED.2021.3076802.

[6] S. Han, S. Yang, R. Li, X. Wu, and K. Sheng, "Current-collapse-free and fast reverse recovery performance in vertical GaN-on-GaN Schottky barrier diode," *IEEE Trans. Power Electron.*, vol. 34, no. 6, pp. 5012–5018, Jun. 2019, doi: 10.1109/TPEL.2018.2876444.

[7] S. Han, S. Yang, and K. Sheng, "High-voltage and high-ION/IOFF vertical GaN-on-GaN Schottky barrier diode with nitridation-based Termination," *IEEE Electron Device Lett.*, vol. 39, no. 4, pp. 572–575, Apr. 2018, doi: 10.1109/LED.2018.2808684.

[8] Z. Bian *et al.*, "Leakage mechanism of quasi-vertical GaN Schottky barrier diodes with ultra-low turn-on voltage," *Appl. Phys. Exp.*, vol. 12, no. 8, Aug. 2019, Art. no. 084004, doi: 10.7567/1882-0786/ab3297.

[9] M. Yutaka, I. Takayuki, K. Yuji, M. Tae, and I. Hirotaka, "Recent progress of large size and low dislocation bulk GaN growth," *Proc. SPIE.*, vol. 11280, Feb. 2020, Art. no. 1128002, doi: 10.1117/12.2540737.

[10] T. Hayashida, T. Nanjo, A. Furukawa, T. Watahiki, and M. Yamamuka, "Leakage current reduction of vertical GaN junction barrier Schottky diodes using dual-anode process," *Jpn. J. Appl. Phys.*, vol. 57, no. 4, Feb. 2018, Art. no. 040302, doi: 10.7567/JJAP.57.040302.

[11] W. Li *et al.*, "Design and realization of GaN trench junction-barrier-Schottky-diodes," *IEEE Trans. Electron Devices*, vol. 64, no. 4, pp. 1635–1641, Apr. 2017.

[12] Y. Zhang *et al.*, "Novel GaN trench MIS barrier Schottky rectifiers with implanted field rings," in *IEDM Tech. Dig.*, Dec. 2016, pp. 10.2.1–10.2.4, doi: 10.1109/IEDM.2016.7838386.

[13] Y. Zhang *et al.*, "Trench formation and corner rounding in vertical GaN power devices," *Appl. Phys. Lett.*, vol. 110, no. 19, May 2017, Art. no. 193506, doi: 10.1063/1.4983558.

[14] S. Chen, H. Chen, Y. Qiu, and C. Liu, "Systematic design and parametric analysis of GaN vertical trench MOS barrier Schottky diode with p-GaN shielding rings," *IEEE Trans. Electron Devices*, vol. 68, no. 11, pp. 3060–3066, Sep. 2021, doi: 10.1109/TED.2021.3109845.

[15] M. Xiao, R. Zhang, D. Dong, H. Wang, and Y. Zhang, "Design and simulation of GaN superjunction transistors with 2-DEG channels and fin channels," *IEEE J. Emerg. Sel. Topics Power Electron.*, vol. 7, no. 3, pp. 1475–1484, Sep. 2019, doi: 10.1109/JESTPE.2019.2912978.

[16] M. Meneghini *et al.*, "GaN-based power devices: Physics, reliability, and perspectives," *J. Appl. Phys.*, vol. 130, no. 18, Nov. 2021, Art. no. 181101, doi: 10.1063/5.0061354.

[17] R. Ghandi, A. Bolotnikov, D. Lilienfeld, S. Kennerly, and R. Ravisekhar, "3 kV SiC charge-balanced diodes breaking unipolar limit," in *Proc. 31st Int. Symp. Power Semiconductor Devices ICs (ISPSD)*, May 2019, pp. 179–182, doi: 10.1109/ISPSD.2019.8757568.

[18] R. Ghandi, A. Bolotnikov, S. Kennerly, C. Hitchcock, P. M. Tang, and T. P. Chow, "4.5 kV SiC charge-balanced MOSFETs with ultra-low on-resistance," in *Proc. 32nd Int. Symp. Power Semiconductor Devices ICs (ISPSD)*, Sep. 2020, pp. 126–129, doi: 10.1109/ISPSD46842.2020.9170171.

[19] M. Xiao *et al.*, "Origin of leakage current in vertical GaN devices with nonplanar regrown p-GaN," *Appl. Phys. Lett.*, vol. 117, no. 18, Nov. 2020, Art. no. 183502, doi: 10.1063/5.0021374.

[20] C. Liu, Y. Cai, H. Jiang, and K. M. Lau, "Monolithic integration of III-nitride voltage-controlled light emitters with dual-wavelength photodiodes by selective-area epitaxy," *Opt. Lett.*, vol. 43, no. 14, pp. 3401–3404, Jul. 2018, doi: 10.1364/OL.43.003401.

[21] Y. Zhang *et al.*, "Vertical GaN junction barrier Schottky rectifiers by selective ion implantation," *IEEE Electron Device Lett.*, vol. 38, no. 8, pp. 1097–1100, Aug. 2017, doi: 10.1109/LED.2017.2720689.

[22] J. Liu *et al.*, "1.2 kV vertical GaN fin JFETs with robust avalanche and fast switching capabilities," in *IEDM Tech. Dig.*, Dec. 2020, p. 23, doi: 10.1109/IEDM13553.2020.9372048.

[23] J. Liu *et al.*, "1.2-kV vertical GaN fin-JFETs: High-temperature characteristics and avalanche capability," *IEEE Trans. Electron Devices*, vol. 68, no. 4, pp. 2025–2032, Apr. 2021, doi: 10.1109/TED.2021.3059192.

[24] H. Yuan *et al.*, "Analytical models of on-resistance and breakdown voltage for 4H-SiC floating junction Schottky barrier diodes," *Solid-State Electron.*, vol. 103, pp. 83–89, Jan. 2015, doi: 10.1016/j.sse.2014.10.004.

[25] H. Huang, J. Huang, H. Hu, J. Cheng, and B. Yi, "Analytical models of breakdown voltage and specific on-resistance for vertical GaN unipolar devices," *IEEE Access*, vol. 7, pp. 140383–140390, 2019, doi: 10.1109/ACCESS.2019.2944028.

[26] T. Maeda *et al.*, "Impact ionization coefficients and critical electric field in GaN," *Jpn. J. Appl. Phys.*, vol. 129, no. 18, Apr. 2021, doi: 10.1063/JJAP.5.0050793.

[27] C. Liu, R. A. Khadar, and E. Matioli, "GaN-on-Si quasi-vertical power MOSFETs," *IEEE Electron Device Lett.*, vol. 39, no. 1, pp. 71–74, Jan. 2018, doi: 10.1109/LED.2017.2779445.

[28] A. Bolotnikov, P. A. Losee, R. Ghandi, S. Kennerly, R. Datta, and X. She, "SiC charge-balanced devices offering breakthrough performance surpassing the 1-D Ron versus BV limit," *Mater. Sci. Forum*, vol. 963, pp. 655–659, Jun. 2019, doi: 10.4028/www.scientific.net/MSF.963.655.

[29] J. Knoll *et al.*, "Characterization of 4.5 kV charge-balanced SiC MOSFETs," in *Proc. IEEE Appl. Power Electron. Conf. Expo. (APEC)*, Jun. 2021, pp. 2217–2223, doi: 10.1109/APEC42165.2021.9487454.